The importance of a surface organic layer in simulating permafrost thermal and carbon dynamics

Elchin Jafarov[1*] and Kevin Schaefer[1]

[1] National Snow and Ice Data Center, Cooperative Institute for Research in Environmental Sciences, University of Colorado at Boulder, Boulder, CO 80309

*Corresponding author, Email: elchin.jafarov@colorado.edu

Abstract

Permafrost-affected soils contain twice as much carbon as currently exists in the atmosphere. Studies show that warming of the perennially frozen ground could initiate significant release of the frozen soil carbon into the atmosphere. To reduce the uncertainty associated with the modeling of the permafrost carbon feedback it is important to start with the observed soil carbon distribution. We initialized frozen carbon using the recent Northern Circumpolar Soil Carbon Dataset. To better address permafrost thermal and carbon dynamics we implemented a dynamic surface organic layer with vertical carbon redistribution. In addition, we introduced dynamic root growth controlled by active layer thickness, which improved soil carbon exchange between frozen and thawed pools. Our results indicate that a dynamic surface organic layer improved permafrost thermal dynamics and simulated thaw depth. These improvements allowed us achieve better agreement with the estimated carbon stocks in permafrost-affected soils using historical climate forcing.

1. Introduction

Warming of the global climate will lead to widespread permafrost thaw and degradation with impacts on ecosystems, infrastructure, and emissions to amplify climate warming (Oberman, 2008; Callaghan et al., 2011, Shuur et al., 2015). Permafrost-affected soils in the high northern latitudes contain 1300±200 Gt of carbon, where about 800 Gt C is preserved frozen in permafrost (Hugeluis et al., 2014). As permafrost thaws, organic matter frozen within permafrost will thaw and decay, which will initiate the permafrost carbon feedback (PCF), releasing an estimated 120±85 Gt of carbon emissions by 2100 (Schaefer et al., 2014). The wide range of estimates of carbon emissions from thawing permafrost depend in large part on the ability of models to simulate present permafrost area extent (Brown et al., 1997). For example, the simulated permafrost in some models is significantly more sensitive to thaw, with corresponding larger estimates of carbon emissions (Koven et al., 2013). Narrowing the uncertainty in estimated carbon emissions requires improvements in how Land Surface Models (LSMs) represent permafrost thermal and carbon dynamics.

The active layer in permafrost regions is the surficial layer overlying the permafrost, which undergoes seasonal freeze-thaw cycles. Active layer thickness (ALT) is the maximum depth of thaw at the end of summer. LSMs used to estimate emissions from thawing permafrost typically assume that the frozen carbon is located in the upper permafrost above 3 meters depth and below the maximum ALT (Koven et al., 2011; Schaefer et al., 2011; MacDougall et al., 2012). Thus, the simulated ALT determines the volume of permafrost in the top 3 meters of soil, and thus the initial amount of frozen carbon. Consequently, any biases in the simulated ALT could influence the initial amount of frozen carbon, even if different models initialize the frozen carbon in the same way. Also, the same thermal biases that lead to deeper simulated active layers also lead to warmer soil temperatures, making the simulated permafrost more vulnerable to thaw and resulting in higher emissions estimates (Koven et al., 2013).

The surface organic layer (SOL) is the surface soil layer of nearly pure organic matter that exerts a huge influence on the thermodynamics of the active layer. The organic layer thickness (OLT) usually varies between 5-30 cm, depending on a balance between the litter accumulation rate relative to the organic matter decomposition rate (Yi et al., 2009; Johnstone et al., 2010). A recent model intercomparision study shows that LSMs need more realistic surface processes such as upper organic layer and better representations of subsoil thermal dynamics (Ekici et al., 2014a). The low thermal conductivity of the SOL makes it an effective insulator decreasing the heat exchange between permafrost and the atmosphere (Rinke et al., 2008). The effect of the SOL has been well presented in several modeling studies. For example, Lawrence and Slater (2008) showed that soil organic matter affects the permafrost thermal state in the Community Land Model (CLM), and Jafarov et al., (2012) discussed the effect of the SOL in the regional modeling study for Alaska, United States. Recently, Chadburn et al., (2015a,b) incorporated the SOL in the Joint UK Land Environment Simulator (JULES) model to illustrate its influence on ALT and ground temperatures both at a site specific study in Siberia, Russia, and globally. In essence, the soil temperatures and ALT decrease as the OLT increases. Consequently, how (or if) LSMs represent the SOL in the simulated soil thermodynamics will simultaneously determine the initial amount of frozen permafrost carbon and the vulnerability of the simulated permafrost to thaw.

Here we describe a fully dynamic SOL to demonstrate the importance of coupling soil biogeochemistry and thermodynamics to improve the simulated permafrost temperature and ALT. We improved the Simple Biosphere/Carnegie-Ames-Stanford Approach (SiBCASA) model (Schaefer et al., 2011) by adding a dynamic SOL and limiting plant growth in frozen soils and demonstrated that these changes improve permafrost thermal and carbon dynamics in comparison. Then we used the modified model to evaluate current permafrost carbon stock

(Hugeluis et al., 2014) under the steady state climate in the early 20th century.

2. Methods

We used the SiBCASA model (Schaefer et al., 2008) to evaluate current soil carbon stocks in permafrost affected soils. SiBCASA has fully integrated water, energy, and carbon cycles and computes surface energy and carbon fluxes at 10 minute time steps. SiBCASA predicts the moisture content, temperature, and carbon content of the canopy, canopy air space, and soil (Sellers et al., 1996a; Vidale and Stockli, 2005). To calculate plant photosynthesis, the model uses a modified Ball-Berry stomatal conductance model (Ball, 1998; Collatz et al., 1991) coupled to a C3 enzyme kinetic model (Farquhar et al., 1980) and a C4 photosynthesis model (Collatz et al., 1992). It predicts soil organic matter, surface litter, and live biomass (leaves, roots, and wood) in a system of 13 prognostic carbon pools as a function of soil depth (Schaefer et al., 2008). The model biogeochemistry does not account for disturbances, such as fire, and does not include a nitrogen cycle. SiBCASA separately calculates respiration losses due to microbial decay (heterotrophic respiration) and plant growth (autotrophic respiration).

SiBCASA uses a fully coupled soil temperature and hydrology model with explicit treatment of frozen soil water originally from the Community Climate System Model, Version 2.0 (Bonan, 1996; Oleson et al., 2004). To improve simulated soil temperatures and permafrost dynamics, Schaefer et al. (2009) increased the total soil depth to 15 m and added the effects of soil organic matter on soil physical properties. Simulated snow density and depth, and thus thermal conductivity, significantly influence simulated permafrost dynamics, so Schaefer et al. (2009) added the effects of depth hoar and wind compaction on simulated snow density and depth. Recent model developments include improved numerical scheme for frozen soil biogeochemistry (Schaefer and Jafarov, 2015).

We spun SiBCASA up to steady-state initial conditions using an input weather dataset from the Climatic Research Unit National Center for Environmental Predictions (CRUNCEP)[1] (Wei et al, 2014) for the entire permafrost domain in the northern hemisphere (Brown et al., 1997). CRUNCEP is modeled weather data at 0.5x0.5 degree latitude and longitude resolution optimally consistent with a broad array of observations. The CRUNCEP dataset used in this study spans 110 years, from 1901 to 2010. We selected the first 30 years from the CRUNCEP dataset (1901 to 1931) and randomly distributed them over 900 years. To run our simulations we used JANUS High Performance Computing (HPC) Center at University of Colorado at Boulder. The 900-yr time span was chosen in order to make optimal use of the computational time, which allowed us to finish one spinup simulation on JANUS HPC without interruptions.

2.1.Frozen carbon initialization

The Permafrost Carbon Network published a revised Northern Circumpolar Soil Carbon Dataset version 2 (NCSCDv2) (Hugeluis et al., 2013). The NCSCDv2 includes soil carbon density maps in permafrost-affected soils available at several spatial resolutions ranging from 0.012^{o} to 1^{o}. The dataset consists of spatially extrapolated soil carbon data from more than 1700 soil core samples. This dataset has three main layers, each 1 meter in depth, distributed between ground surface and 3 meter depth.

We placed the frozen carbon within the top three meters of simulated permafrost, ignoring deltaic and loess deposits that are known to extend well beyond 3 meters of depth (Hugelius et al., 2014). The bottom of the permafrost carbon layer is fixed at 3 meters, while the

[1] ftp://nacp.ornl.gov/synthesis/2009/frescati/temp/land_use_change/original/readme.htm

top varies spatially with changes in ALT during the spinup run. Defining the permafrost table as the maximum ALT, we essentially assume that the soil above the permafrost table has thawed frequently enough over thousands of years to decay away all the old carbon.

We initialized frozen carbon between the permafrost table and 3 meters depth using two scenarios: 1) spatially uniform distribution of the frozen carbon throughout the permafrost domain (Schaefer et al., 2011), and 2) observed distribution of the frozen carbon according to the NCSCDv2. It is important to know the "stable" depth of the active layer before initializing frozen carbon. We run the model for several years in order to calculate ALT, and then initialized frozen carbon below the maximum calculated ALT. The frozen carbon was initialized only once during the first equilibrium run cycle. For the next equilibrium run we used the previously calculated permafrost carbon. We defined an equilibrium point when changes in overall permafrost carbon were negligible or almost zero.

The total initial frozen carbon in each soil layer between the permafrost table and 3 meters is

$$C_{fr}^{i} = \rho_c \Delta z_i, \tag{1}$$

where C_{fr}^{i} is the total permafrost carbon within the i^{th} soil layer, ρ_c is the permafrost carbon density, and Δz_i is the thickness of the i^{th} soil layer in the model. For the uniform permafrost carbon distribution, ρ_c =21 kg C m^{-3} assumed to be spatially and vertically uniform(Schaefer et al., 2011). For the observed distribution from the NCSCDv2, ρ_c varies both with location and depth (Hugeluis et al., 2013).

The carbon in each layer is divided into three pools as follows:

$$C^i_{slow} = 0.8C^i_{fr}$$
$$C^i_{met} = 0.2f_{root2met}C^i_{fr} \quad (2)$$
$$C^i_{str} = 0.2f_{root2strt}C^i_{fr},$$

where $f_{root2met}$ and $f_{root2strt}$ are the simulated fractions of root pool losses to the soil metabolic and structural pools respectively (Schaefer et al., 2008). The nominal turnover time is 5 years for the slow pool, 76 days for the structural pool, and 20 days for the metabolic pool. Schaefer et al. (2011) has a 5% loss to the metabolic pool and a 15% loss to the structural pool based on observed values in Dutta et al. (2006). The simulated fractions are actually 5.6% to the metabolic pool and 14.4% to the structural pool. We found it encouraging that the numbers calculated with the SiBCASA metabolic fractions resulted in numbers that are close to the observed values in Dutta et al. (2006).

2.2. Dynamic SOL

We modified SiBCASA to include a dynamic SOL by incorporating the vertical redistribution of organic material associated with soil accumulation. SiBCASA calculates the soil physical properties as a weighted average of those of organic matter, mineral soil, ice and water (Schaefer et al., 2009). The physical properties include soil porosity, hydraulic conductivity, heat capacity, thermal conductivity, and matric potential. The model calculates the organic fraction used in the weighted mean as the ratio of simulated carbon density to the density of pure organic matter. SiBCASA does not account for the compression of organic matter. Since the prognostic soil carbon pools vary with depth and time, the organic fraction and the physical properties all vary with time and depth. We only summarized these calculations here since the calculations are covered in detail in Schaefer et al. (2009).

Each model layer has a complete set of prognostic soil carbon pools. The previous version of the model distributed fine and coarse root growth vertically within the soil column based on observed root distributions. As the roots die, carbon is transferred to the soil carbon pools for that layer. Thus, the maximum rooting depth determined the maximum depth of 'current' or 'active' carbon in the model. Of course, if the maximum rooting depth fell below the permafrost table, the model would accumulate permafrost carbon. The current version of the model initializes the permafrost carbon by assigning carbon to the soil carbon pools below the maximum thaw depth. These frozen pools remained inactive until the layer thaws. As live, above-ground biomass in the model dies, carbon is transferred into the first layer as litter. Without the vertical redistribution we describe here to create a surface organic layer, the top layer of the model tended to accumulate carbon in excess of that expected for pure organic matter.

To allow vertical movement and build up a SOL, we placed a maximum limit on the amount of organic material that each soil layer can hold. When the simulated carbon content exceeds this threshold, the excess carbon is transferred to the layer below. This is a simplified version of the Koven et al., (2009) carbon diffusion model, which accounts for all sedimentation and cryoturbation processes, while we wanted to limit our model only to the buildup of a SOL.

We calculate the maximum allowed carbon content per soil layer, C_{max}, as

$$C_{max} = \rho_{max} \Delta z \frac{1000}{MW_C}, \quad (3)$$

where ρ_{max} is the density of pure organic matter or peat, Δz is the soil layer thickness (m), MW_C is the molecular weight of carbon (12 g mol^{-1}), and the factor of 10^3 converts from grams to kilograms. Based on observations of bulk densities of peat, we assume ρ_{max}, is 140 kg m^{-3}

(Price et al., 2005). The MW_C term converts the expression into mol C m^{-2}, the SiBCASA internal units for carbon. The simulated organic soil fraction per soil layer, f_{org}, is defined as

$$f_{org} = \frac{C}{C_{max}}, \tag{4}$$

where C is the carbon content per soil layer (mol m^{-2}). To convert to carbon we assume that the fraction of organic matter is 0.5, which means that half of the organic matter by mass is carbon. The original formulation allowed f_{org} to exceed 1.0 such that the excess organic material was essentially 'compressed' into the top soil layer, resulting in a 2-cm simulated SOL. We place an upper limit of 0.95 on f_{org} and transfer the excess carbon to the layer below. The OLT is defined as the bottom of the lowest soil layer where f_{org} is 0.95.

2.3. Root growth and soil thermal factor

Fine roots supply nutrients and water for photosynthesis, so essentially the leaves and roots together define the photosynthetic capacity of the plant. Plants have optimized carbon allocation to grow only enough fine roots to properly supply the leaves with the correct amount of water and nutrients to support photosynthesis. So, as plants grow new leaves, they also grow new fine roots to supply them with nutrients and water. Linking root growth to leaf growth is a convenient and simple way to represent this coupling in SiBCASA.

Here we take this coupling one step further and recognize that frozen soil reduces the plant photosynthetic capacity and regulates root and leaf growth. Plants cannot photosynthesize in frozen soil. Frozen soil in the root zone reduces the photosynthetic capacity of the plant by limiting the water available for photosynthesis. Roots cannot grow while soil is frozen and if roots can't grow, leaves can't grow. The changes we implement link soil thermodynamics to root growth, leaf growth, and plant photosynthesis.

In the original formulation (without a dynamic SOL), plant photosynthesis, leaf growth, and fine root growth were controlled primarily by near surface air temperature: when the near surface air temperature exceeded 0^{o}C, leaves and roots started to grow. SiBCASA assumes fine root growth decreases exponentially with depth based on observed vertical root distributions (Schaefer et al., 2008) with 90% of fine root growth occurring in the top 1 meter of soil. Consequently, the vertical distribution of new root growth between the soil layers is prescribed using exponential curve fits to observed vertical root distributions. Before the changes we describe here, the maximum rooting depth sometimes exceeded the thaw depth in permafrost soils, resulting in root growth directly in permafrost, which resulted in false permafrost carbon accumulation since growing roots cannot penetrate frozen soil. The roots that grew into the permafrost never thawed and soon died, but never decayed, resulting in an unrealistic buildup of carbon in the upper layers of permafrost. This, in turn, set up a feedback where the unrealistic increase in organic matter in the simulated permafrost changed the thermodynamic properties and decreased the ALT, resulting in additional carbon buildup. To solve this problem, we kept the original exponential vertical rooting profile, but set maximum rooting depth equal to the thaw depth. This allowed the maximum rooting depth to vary with time and effectively restricted all root growth to within the thawed portion of the active layer.

Soil thaw always lags behind warming of the canopy. Photosynthesis is limited by water availability as well as canopy temperature and starts later in spring after the surface soil layers thaw out. Before the changes described below, leafout and new root growth occurred as many as 60 days before the start of photosynthesis. In reality, leafout, root growth, and the start of photosynthesis should occur at the same time.

We synchronized leafout, root growth, and photosynthesis by restricting root growth to occur only in thawed soil layers. In SiBCASA, leaf growth is linked to fine root growth (Schaefer et al., 2008), so this also delays spring leafout until the soil begins to thaw. We first calculated the fraction of thawed roots:

$$R_{th} = \sum_{k=1}^{nroot} R_f(1 - F_{ice}), \quad (6)$$

where R_{th} is the fraction of total roots that are thawed, *nroot* is the deepest soil layer with roots, R_f is the reference root fraction per soil layer based on observed root distributions (Jackson et al., 1996), and F_{ice} is the ice fraction per soil layer. F_{ice} is calculated from the liquid water and ice content of each soil layer, both of which are prognostic variables, accounting for latent heat effects. F_{ice} varies from zero for a completely thawed soil layer to one for a completely frozen soil layer. This assumes that water in each layer is evenly distributed such that F_{ice} equals the frozen fraction.

Restricting root growth within the thawed portion of the active layer results from the fact that roots cannot penetrate frozen soil. Root growth still decreases exponentially with depth, but we used an effective rooting depth equal to the thaw depth or the theoretical maximum rooting depth from the observed vertical root distributions (whichever is less). We calculated an effective root fraction R_{eff}, to control the vertical distribution of new growth carbon within the soil column:

$$R_{eff} = R_f(1 - F_{ice})/R_{th}. \quad (8)$$

Dividing by R_{th} ensures that R_{eff} sums to one within the soil column, which essentially ensures that all new root growth is distributed only within the thawed portion of the soil column. Here, we replaced R_f with R_{eff} in the vertical distribution of coarse woody roots in the wood pool and the fine roots in the root pool and associated calculations of autotrophic respiration.

To synchronize growth primary productivity (GPP) with leafout, we treated the reference vertical root distribution, R_f, as the potential root growth defining the maximum potential GPP. Since the sum of R_f is always one, when $R_{th} < 1$, GPP must be less than its full potential. We defined a GPP scaling factor, $S_{soilfrz}$, as

$$S_{soilfrz} = \begin{cases} R_{th} & \text{for } R_{th} \geq 0.01 \\ 0 & \text{for } R_{th} < 0.01 \end{cases}. \quad (7)$$

This assumes that at least 1% of the roots must be thawed for GPP to occur, corresponding to about ~1 cm of thawed soil. $S_{soilfrz}$ is applied along with the soil moisture and canopy temperature scaling factors to constrain photosynthesis while soil is frozen (Schaefer et al., 2008). To constrain wood growth, we applied $S_{soilfrz}$ to the temperature scaling factors to the decay rate constant that controls wood growth

$$k_{eff} = S_{nsc} S_T S_M S_{frost} S_{soilfrz} k_{wood}, \quad (9)$$

where k_{eff} is the effective growth rate, S_{nsc} is the non-structural carbohydrate scaling factor, S_T is the canopy temperature scaling factor, S_{frost} is the frost inhibition function, and k_{wood} is the reference wood growth rate. S_T, S_{frost}, and $S_{soilfrz}$ are the same scaling factors that control GPP under the assumption that the factors that control photosynthesis also control wood growth (Schaefer et al., 2008). This is also consistent with what we normally see in discontinuous permafrost zones: trees cannot grow in shallow permafrost. Indeed, one can often detect the presence of permafrost in the discontinuous zone simply by noting the lack of trees.

To constrain leaf growth, we added $S_{soilfrz}$ to the frozen leaf scaling factor

$$S_{leaffrz} = S_{soilfrz} / \left(1 + exp\left(1.3(273 - T_{can})\right)\right), \quad (10)$$

where $S_{leaffrz}$ is the frozen leaf scaling factor and T_{can} is canopy temperature.

3. Results

The dynamic SOL decreased the simulated ALT on average 50% across the domain and allowed the model to simulate permafrost in discontinuous zones where it could not before (Figure 1). The area of near surface permafrost simulated with the current version of the model equals to 13.5 mil km^2 which is almost 38% greater than without the dynamic SOL (Schaefer et al., 2011). This area is closer to the observation from the International Permafrost Association which is about 16.2 mil km^2 (Brown et al.,1997). Simulated ALT less than 2 m covers about 92% of the area in the new simulations (Figure 1B) in comparison to 66% of the area in the Schaefer et al. (2011) simulations (Figure 1A). The previous version of SiBCASA could not simulate permafrost in many parts of the discontinuous zone with relatively warm climate. Adding the dynamic SOL essentially decreased the thermal conductivity of the surface soil to allow SiBCASA to simulate permafrost where the mean annual air temperatures (MAAT) are close to 0 °C.

To illustrate the improvement of the simulated ALT with respect to the observed data, we compared simulated ALT with measured values from Circumpolar Active Layer Monitoring (CALM) stations. The CALM network is a part of the Global Terrestrial Network for Permafrost (GTN-P) (Burgess et al., 2000). The monitoring network measures ALT either using a mechanical probe or a vertical array of temperature sensors (Brown et al., 2000; Shiklomanov et al., 2010). After matching up the CALM coordinates with the coordinates of previously simulated ALT (Schaefer et al., 2011), we excluded sites with no measurements or ALT greater than 3m depth, ending up with 76 CALM stations. Figure 2 shows simulated vs. observed ALT for the 76 CALM sites. The current simulations have a higher resolution than Schaefer et al. (2011) simulations, which allowed us to reach a higher order of heterogeneity between measured and simulated ALTs. The Pearson's correlation coefficient, R, is negative and not significant for the Schaefer et al. (2011) simulations (Figure 2A), but is positive and statistically significant for the current simulations assuming $p < 0.05$ (Figure 2B). The dynamic SOL greatly improves the simulated ALT, but SiBCASA still tends to overestimate ALT.

Figure 3 illustrates the effect of the frozen soil restrictions on phenology and GPP at a single point in central Siberia. Before applying a frozen soil restriction, SiBCASA maintained fine roots even in winter, resulting in root growth all year with a peak in spring corresponding to simulated leafout (Figure 3A). Simulated GPP was restricted by liquid water availability and was closely tied to thawing of the active layer, resulting in a lag as high as 60 days between leafout and start of GPP in spring. Restricting growth and GPP to when the soil is thawed essentially synchronizes all phenological events to occur at the same time (Figure 3B).

In the previous version without a dynamic SOL the ALT was generally deep in forest biomes, but in the new version there is a thick SOL (due to high GPP), which leads to a shallower ALT. Without restricting root growth within only thawed part of the soil the shallower ALT feedback leads to a significant amount of root growth in the permafrost itself, which puts carbon directly into the permafrost stores. This is unrealistic since growing roots cannot penetrate frozen soil, so the frozen soil restrictions on GPP and root growth together eliminate this problem.

Restricting growth and GPP to when the soil is thawed delayed the onset of plant photosynthesis in spring in permafrost-affected regions. Introduction of the thawed root fraction in the model reduced GPP primarily in early spring. To illustrate the difference between unconstrained and restricted root growth (Figure 3), we ran the model for ten years for both cases. The difference between unconstrained and restricted root growth cases (Figure 4) indicates an overall ~9% reduction in GPP for the entire permafrost domain, nearly all of which occurred in spring.

To illustrate soil carbon distribution with depth we selected three representative areas: a continuous permafrost area corresponding to tundra type biome above the Arctic circle, an area in the boundary of continuous and discontinuous permafrost corresponding to the boreal forest biome, and an area near the south border of the discontinuous permafrost corresponding to poorly vegetated-rocky areas. We calculated mean and standard deviation of the carbon density distribution with depth for 200 grid points around each of the three selected locations. Simulated typical carbon densities from selected locations are shown on Figure 5. All profiles shown on Figure 5 show a similar pattern: a 20-30 cm SOL with reduced carbon content at the bottom of the active layer. In contrast, the observed vertical carbon profiles show fairly uniform carbon density with depth throughout the active layer and into the permafrost Harden et al., (2012). SiBCASA lacks the cryotubation processes such as cryotic mixing that would redistribute carbon within the active layer. As a result, the carbon at the bottom of the active layer decayed and respired away during spinup.

The decrease in ALT resulting from a dynamic SOL increases the volume of permafrost in the top 3 meters of soil, greatly increasing the initial amount of frozen permafrost carbon in the simulations. Schaefer et al. (2011) without the dynamic SOL assumed a uniform permafrost carbon density of 21 $kg \cdot C \cdot m^{-3}$, resulting in a total of 313 Gt of permafrost carbon at the start of their transient run (Figure 6A). To compare with the Schaefer et al. [2011] results, we initialized the permafrost carbon using the same assumed uniform carbon density and ran

SiBCASA to steady state initial conditions (Figure 6B). Assuming the same uniform carbon density, the current version with the dynamic SOL results in a total of ~680Gt C compared to 313 GtC in Schaefer et al. (2011). The dynamic SOL effectively doubled the volume of permafrost in the top three meters of soil and the amount of simulated frozen carbon.

Prescribing permafrost carbon according to the NCSDC dataset allowed us to better match with the observed pattern in the soil carbon. However, it is does not mean that after the spinup simulated permafrost carbon stocks exactly matched the NCSDC data. During spinup, ALT varies with time, introducing carbon movement from frozen to thawed pools. In discontinuous zones, if the model simulated permafrost, it tended to produce a deeper ALT and thus less permafrost carbon than the NCSCD. The major difference between uniform frozen carbon initialization (Fig 7A) and initialization according to the NCSCD (Fig 7B) is that SiBCASA simulated permafrost in more places. However, the NCSCD map (Fig 7B) shows that not all frozen soil contains a uniform amount of frozen carbon. Therefore simulating 'correct' ALT is important and should improve the overall permafrost carbon storage.

Initializing SiBCASA with the observed spatial distribution of permafrost carbon from the NCSCDv2 resulted in ~560 GtC of carbon stored in permafrost after spinup. SiBCASA underestimated the SOC in the Eastern Canada and Western Siberia, and overestimated SOC in Central Siberia (Figure 7A and B). Failure to simulate soil carbon in southeast Canada and southwest Siberia (Figure 7C) could be attributed to deep active layer thickness. The overestimation of SOC in Central Siberia is a result of coupling between GPP and ALT. The overall amount of soil frozen carbon is less than that calculated assuming uniform frozen carbon distribution. It is important to note that the SOL, ALT, and the permafrost thickness are the same for both cases (Figure 7A and B). This is due to the fact that in both cases soil carbon is added in the permafrost layer below the active layer. Consequently, the amount of soil carbon in the active layer stays does not change between simulations and has the same thermal and carbon dynamics, and thus ALT. The smaller permafrost carbon stock simulated for the non-uniform case is mainly due to the fact that we did not initialize frozen carbon in regions where according to the NCSCDv2 it is not present, such as the Brooks Range in Alaska.

4. Discussion

The dynamic SOL insulates ALT from air temperature, allowing SiBCASA to simulate permafrost in many discontinuous permafrost regions where it could not before. This result complements similar findings by Lawrence and Slater (2008), Yi et al., (2009), Ekici et al., (2014b), and Chadburn et al., (2015a,b), when changes in thermal properties associated with the presence of soil organic matter cooled the ground. In southeastern Canada and southwestern Siberia, SiBCASA simulates ALT up to 3 meter, and therefore almost no frozen carbon. For example, observed mean annual ground temperatures within southeast Canada region ranges from below to above 0 ^{o}C (Smith, and Burgess, 2000), which suggests that the actual permafrost distribution and associated ALT in these regions would be highly heterogeneous. Models like SiBCASA cannot capture such sub-grid heterogeneity, resulting in a deeper, uniform ALT across the grid cell.

To address the effect of different environmental factors we correlated ALT with near surface air temperature (NSAT), down-welling long-wave radiation (DLWR), snow depth (SND), and soil wetness fraction (SWF). The NSAT has a significant effect on the ALT (Camill 2005, Gallaghan et al., 2011). To show this influence, we averaged NSAT in early fall, for two months September and October over 10 years (Figure 8A). The areas with deep ALT (Figure 1B) fall into the regions where NSATs are greater than one degree centigrade and greater than 5 ^{o}C in the south-east Canada. Figure 9A shows the correlation between NSAT and ALT, which indicates clear relation between NSAT and ALT.

The DLWR averaged over 10 years showed higher radiation along the south boundaries of the domain, in particular southeast Canada and southwest Siberia (Figure 8B). The effect of the DLWR on the ALT is more scattered as opposed to NSAT (Figure 9B). However, in general it showed behaviour similar to NSAT.

SND is another important factor contributing to the permafrost thermal state. Zhang (2005) indicates that SND less than 50cm have the greatest impact on soil temperatures. Figure 8C shows maximum simulated snow depth calculated over the last 10 years of the steady state run. The snow effect on the soil thermal state is less obvious and highly dependent on different physical processes, such as wind, snow metamorphism, and depth hoar formation (Sturm et al., 1997). Ekici et al., (2014) confirm nonlinear behavior of snow after modeling soil temperatures for four sites using six CLM model. Similarly, Jafarov et al., (2014) shows that snow thermal properties not always regulated by the SND. Figure 9C also indicate no correlation with ALT.

Figure 8D shows an averaged soil wetness map, which indicates high SWF in both regions where model simulates deep ALT. This suggests that SOL does not provide enough protection for permafrost in regions with wet soils and mild air temperatures, which complements similar funding by Lawrence and Slater (2008). The calculated partial correlation between SWF and ALT indicate a clear relationship between them. Figure 9D confirms this statement showing that wetter soils associated with higher ALT.

Before implementing the dynamic SOL, the maximum rooting depth only occasionally fell below the permafrost table. However, after implementing the dynamic SOL, the simulated ALT decreased and new root growth was placed directly into the permafrost with no chance to decay. This phenomenon occurred primarily in the mixed deciduous evergreen forest in south-central Siberia and resulted in a long-term carbon sink into the permafrost carbon pool. It resulted from the fact that the maximum rooting depth determined by the fixed, exponential root distribution incorrectly extended into the permafrost. In permafrost-affected soils, seasonal root growth is largely regulated by the soil thermal conditions (Tryon and Chapin 1983, Van Cleve et al., 1983). Therefore in the LSMs it is important to restrict root growth to thawed soil layers only. Moreover, previous studies showed that the date of snowmelt usually determines the start date of the growing season and the start of active layer thawing (Grøndahl et al. 2007; Wipf and Rixen 2010). Restricting GPP and all growth using the scaling factors described above synchronizes the simulated start of the growing season.

The ability of the ecosystem and climate models to reproduce the current observed frozen soil carbon distribution is important and could reduce uncertainty associated with modeling of the permafrost carbon feedback. Simulated permafrost vulnerability is tightly coupled with the accurate modeling of the present permafrost distribution, which depends on soil thermal properties. We calculate soil thermal properties based on prognostic soil carbon and soil texture from the Harmonized World Soil Database (HWSD) (FAO et al., 2009). Observations indicate that soils in the southeast Canada have high soil carbon as a result of a large number of peat lands (Hugelius et al., 2014). Peat has low thermal conductivity and could preserve permafrost even at NSATs about zero degrees centigrade (Jafarov et al., 2012) even if the surrounding areas do not have permafrost. However, the HWSD input data does not have enough soil carbon in the southeast Canada and southwest Russia, as a result, we could not simulate permafrost in those regions.

Including dynamic SOL in the model allows us to study the interaction of plant dynamics and soil thermodynamics. In addition it allows us to study other processes in the future, such as fire impacts on soil thermodynamics and recovery from fire, both of which are strongly influenced by the changes in the SOL (Jafarov et al., 2013). For example, Yuan et al., (2012) evaluated the role of wildfire in soil thermal dynamics and ecosystem carbon in Yukon River Basin of Alaska using Terrestrial Ecosystem Model (Yi et al., 2010), showing wildfires and climate change could substantially alter soil carbon storage. The current version of the model does not include the effects of fire, which means that topsoil carbon stays in the system and provides resilience to permafrost. However, in reality, upper SOL could be removed by fire, which would alter soil thermal properties and perturb permafrost carbon stability.

5. Conclusion

Presence of the SOL improves the permafrost thermal dynamics by reducing heat exchange between near surface atmosphere and subsurface. Similarly, to Koven et al., (2009) we show that inclusion of the surface carbon layer dynamics into the model leads to an improved agreement with the estimated carbon stocks in permafrost-affected soils. However, to better simulate known permafrost distribution in the discontinuous permafrost zone it is important to know the exact thickness of the upper soil organic layer. Our setup does not include thick organic layer along the southeastern boundaries of the permafrost domain in Canada as well as southwestern part of Russia, which did not allow the model to simulate permafrost in those regions.

The simplified scheme of the soil carbon dynamics improves permafrost resilience, but does not fully reproduce observed carbon distribution with depth (Harden et al., 2012). The dynamic SOL and rooting depth strengthens the feedback between GPP and ALT (Koven et al., 2009). Higher GPP produces greater litter fall, which increases the input soil carbon at the surface and results in a thicker SOL. The dynamic SOL changes the properties of the near surface soil, resulting in a shallower ALT and cooler soil temperatures. The dynamic rooting depth accounts for a shallower ALT and modulates GPP accordingly. The cooler soil temperatures slow microbial decay and increase the carbon accumulation rate, which in turn increases the SOL and reduces ALT further. Eventually, this feedback results in the development of a peat bog. The changes we describe here indicate that SiBCASA can simulate the dynamics of peat bog development, but the model does not yet include a dynamic vegetation model to account for conversions between biome types, such as boreal forest to peat bog.

6. Acknowledgements

This research was funded by NOAA grant NA09OAR4310063 and NASA grant NNX10AR63G. This work utilized the Janus supercomputer, which is supported by the National Science Foundation (award number CNS-0821794) and the University of Colorado Boulder. We thank K. Gregory at NSIDC for reviewing the manuscript. Software tools used in this study include m_map MATLAB package and shadedErrorBar.m MATLAB script.

7. References

Ball, J. T.: An analysis of stomatal conductance, Ph.D. thesis, Stanford Univ., Stanford, Calif., 1988

Bonan, G. B.: A Land Surface Model (LSM Version 1.0) for ecological, hydrological, and atmospheric studies: Technical description and users guide, NCAR Tech. Note NCAR/TN-417+STR, Natl. Cent. for Atmos. Res., Boulder, Colo., 1996.

Brown, J., K. Hinkel and F. Nelson.: The 1 Circumpolar Active Layer Monitoring (CALM) program: Research designs and initial results. *Polar Geography*, 24,165-258, doi:10.1080/10889370009377698. 2000.

Brown, J., O. J. Ferrians Jr., J. A. Heginbottom, and E. S Melnikov, Eds.: Circum-Arctic Map of Permafrost and Ground-Ice Conditions. U.S. Geological Survey in Cooperation with the Circum-Pacific Council for Energy and Mineral Resources, Circum-Pacific Map Series CP-45, scale 1:10,000,000, 1 sheet, 1997

Brown, J., Hinkel, K.M.; Nelson, F.E.: The circumpolar active layer monitoring (CALM) program: Research designs and initial results. *Polar Geog.*, *24*, 165–258, 2000.

Bonan, G. B.: A Land Surface Model (LSM Version 1.0) for ecological, hydrological, and atmospheric studies: technical description and users guide. NCAR Technical Note NCAR/TN-417+STR, Boulder, Colorado. 1996.

Burgess, M.M.; Smith, S.L.; Brown, J.; Romanovsky, V.; Hinkel, K. The Global Terrestrial Network for Permafrost (GTNet-P): Permafrost Monitoring Contributing to Global Climate Observations. Available online: http://ftp2.cits.rncan.gc.ca/pub/geott/ess_pubs/211/211621/cr_2000_e14.pdf.

Burke, EJ, IP Hartley, and CD Jones.: Uncertainties in the global temperature change caused by carbon release from permafrost thawing, *Cryosphere*, 6, 1063–1076, doi:10.5194/tc-6-1063-2012, 2012

Camill, P: Permafrost thaw accelerates in boreal peatlands during late-20th century climate warming Clim. Change 68 135–52. 2005

Callaghan, T.V., Johansson, M., Anisimov, O., Christiansen, H.H., Instanes, A., Romanovsky, V., and Smith, S.: Chapter 5: Changing permafrost and its impacts. In: Snow, Water, Ice and Permafrost in the Arctic (SWIPA) 2011. Arctic Monitoring and Assessment Programme (AMAP), Oslo, pp 62. 2011.

Chadburn, S., Burke, E., Essery, R., Boike, J., Langer, M., Heikenfeld, M., Cox, P., and Friedlingstein, P.: An improved representation of physical permafrost dynamics in the JULES land surface model, Geosci. Model Dev. Discuss., 8, 715–759, doi:10.5194/gmdd-8-715-2015, 2015a.

Chadburn, S. E., Burke, E. J., Essery, R. L. H., Boike, J., Langer, M., Heikenfeld, M., Cox, P. M., and Friedlingstein, P.: Impact of model developments on present and future simulations of permafrost in a global land-surface model, The Cryosphere Discuss., 9, 1965-2012, doi:10.5194/tcd-9-1965-2015, 2015b.

Collatz, G. J., J. T. Ball, C. Grivet, and J. A. Berry.: Physiological and environmental regulation of stomatal conductance, photosynthesis, and transpiration: A model that includes a laminar boundary layer, Agric. For. Meteorol., 54, 107– 136, doi:10.1016/0168-1923(91)90002-8, 1991.

Collatz, G. J., M. Ribascarbo, and J. A. Berry.: Coupled photosynthesis-stomatal conductance model for leaves of C4 plants, Aust. J. Plant Physiol., 19(5), 519–538, 1992.

Dutta, K., Schuur, E. A. G., Neff, J. C. and Zimov, S. A.: Potential carbon release from permafrost soils of Northeastern Siberia. *Global Change Biol*. 12, 2336–2351, 2006.

FAO, IIASA, ISRIC, ISS-CAS, and JRC: Harmonized World Soil Database (version 1.1) FAO, Rome, Italy and IIASA, Laxenburg, Austria, 2009.

Ekici, A., Chadburn, S., Chaudhary, N., Hajdu, L. H., Marmy, A., Peng, S., Boike, J., Burke, E., Friend, A. D., Hauck, C., Krinner, G., Langer, M., Miller, P. A., and Beer, C.: Site-level model intercomparison of high latitude and high altitude soil thermal dynamics in tundra and barren landscapes, The Cryosphere Discuss., 8, 4959-5013, doi:10.5194/tcd-8-4959-2014, 2014a.

Ekici, A., Beer, C., Hagemann, S., Boike, J., Langer, M., and Hauck, C.: Simulating high-latitude permafrost regions by the JSBACH terrestrial ecosystem model, Geosci. Model Dev., 7, 631-647, doi:10.5194/gmd-7-631-2014, 2014b.

Farquhar, G. D., S. von Caemmerer, and J. A. Berry.: A biochemical model of photosynthetic CO2 assimilation in leaves of C3 species, Planta, 149, 78–90, doi:10.1007/BF00386231, 1980.

Grøndahl L, Friborg T, Soegaard H.: Temperature and snow-melt controls on interannual variability in carbon exchange in the high Arctic. Theor Appl Climatol 88(1):111–125, 2007.

Harden, J. W., Koven, C., Ping, C., Hugelius, G., McGuire D. A., Camill, P., Jorgenson, T., Kuhry, P., Michaelson, G. J., O'Donnell, J.A., Schuur, E. A. G., Tarnocai C., Johnson, K., Grosse, G.: et al. (2012), Field information links permafrost carbon to physical vulnerabilities of thawing, Geophys. Res. Lett., 39, L15704, doi:10.1029/2012GL051958.

Hugelius, G., Strauss, J., Zubrzycki, S., Harden, J. W., Schuur, E. A. G., Ping, C.-L., Schirrmeister, L., Grosse, G., Michaelson, G. J., Koven, C. D., O'Donnell, J. A., Elberling, B., Mishra, U., Camill, P., Yu, Z., Palmtag, J., and Kuhry, P.: Estimated stocks of circumpolar permafrost carbon with quantified uncertainty ranges and identified data gaps, Biogeosciences, 11, 6573–6593, doi:10.5194/bg-11-6573-2014, 2014.

Hugelius, G., Tarnocai, C., Broll, G., Canadell, J. G., Kuhry, P., and Swanson, D. K.: The Northern Circumpolar Soil Carbon Database: spatially distributed datasets of soil coverage and soil carbon storage in the northern permafrost regions, Earth Syst. Sci. Data, 5, 3–13, doi:10.5194/essd-5-3-2013, 2013.

Jafarov E E, Marchenko S S and Romanovsky V E.: Numerical modeling of permafrost dynamics in Alaska using a high spatial resolution dataset, Cryosphere, 6, 613–24, 2012.

Jafarov E.E., Nicolsky D.J., Romanovsky V.E., Walsh J.E., Panda S.K., Serreze M.C. 2014. The effect of snow: How to better model ground surface temperatures. Cold Regions Science and Technology, Volume 102, Pages 63-77, ISSN 0165-232X, doi: 10.1016/j.coldregions.2014.02.007.

Jafarov, E. E., Romanovsky V. E., Genet, H., McGuire A., D., Marchenko, S. S.: The effects of fire on the thermal stability of permafrost in lowland and upland black spruce forests of interior Alaska in a changing climate, Environmental Research Letters, 8, 035030, 2013.

Jackson, R. B., J. Canadell, J. R. Ehleringer, H. A. Mooney, O. E. Sala, and E. D. Schulze.: A global analysis of root distributions for terrestrial biomes, Oecologia, 108, 389–411, doi:10.1007/BF00333714, 1996.

Johnstone J F, Chapin F S III, Hollingsworth T N, Mack M C, Romanovsky V and Turetsky M.:

Fire, climate change, and forest resilience in interior Alaska Can. J. For. Res.40 1302–12, 2010.

Koven, C., P. Friedlingstein, P. Ciais, D. Khvorostyanov, G. Krinner, and C. Tarnocai.: On the formation of high-latitude soil carbon stocks: Effects of cryoturbation and insulation by organic matter in a land surface model, *Geophys. Res. Lett*., 36, L21501, doi:10.1029/2009GL040150, 2009.

Koven, CD, B Ringeval, P Friedlingstein, P Ciais, P Cadule, D Khvorostyanov, G Krinner, and C Tarnocai.: Permafrost carbon-climate feedbacks accelerate global warming, *Proc. Natl. Acad. Sci. USA*, 108(36), 14769–14774, doi/10.1073/pnas.1103910108, 2011.

Koven, C.D., W.J. Riley, and A. Stern.: Analysis of permafrost thermal dynamics and response to climate change in the CMIP5 earth system models. J. Climate. 26:1877–1900. doi:10.1175/JCLI-D-12–00228.1, 2013.

Lawrence, D. M., and A. G. Slater.: Incorporating organic soil into a global climate model. *Climate Dynamics* 30(2-3): 145-160, doi:10.1007/s00382-007-0278-1, 2008.

MacDougall, AH, CA Avis and AJ Weaver.: Significant contribution to climate warming from the permafrost carbon feedback, *Nature Geosci*., 5, 719-721, DOI: 10.1038/NGEO1573, 2012.

Oberman, N.G.: Contemporary Permafrost Degradation of Northern European Russia. In: *Proceedings Ninth International Conference on Permafrost*. Vol. 2, 1305-1310 pp, 2008.

Oleson, K.W.,Dai,Y., Bonan, G., Bosilovich,M., Dickinson, R., and coauthors.: Technical description of the Community Land Model (CLM). NCAR Tech. Note, TN-461+STR, 174 pp, 2004.

Price, J. S., J. Cagampan, and E. Kellner.: Assessment of peat compressibility: is there an easy way? *Hydro. Processes*, 19, 3469–3475, 2005.

Sellers, PJ, DA Randall, GJ Collatz, JA Berry, CB Field, DA Dazlich, C Zhang, GD Collelo, L Bounoua.: A Revised Land Surface Parameterization of GCMs, Part I: Model Formulation, *J. Clim*., *9*(4), 676-705, 1996.

Schaefer, K., Collatz, G. J., Tans, P., Denning, A. S., Baker, I. and co-authors. : The combined Simple Biosphere/Carnegie-Ames-Stanford Approach (SiBCASA) Model. *J. Geophys. Res*., 113, doi:10.1029/2007JG000603, 2008.

Schaefer, K. and Jafarov, E.: A parameterization of respiration in frozen soils based on substrate availability, Biogeosciences Discuss., 12, 12027-12059, doi:10.5194/bgd-12-12027-2015, 2015.

Schaefer, K., T. Zhang, L. Bruhwiler, and A. P. Barrett.: Amount and timing of permafrost carbon release in response to climate warming, *Tellus Series B: Chemical and Physical Meteorology*, DOI: 10.1111/j.1600-0889.2011.00527.x, 2011.

Schaefer, K., Zhang, T., Slater, A. G., Lu, L., Etringer, A. and Baker, I.: Improving simulated soil temperatures and soil freeze/thaw at high-latitude regions in the Simple Biosphere/Carnegie-Ames-Stanford Approach model. *J. Geophys. Res.*, 114, doi:10.1029/2008JF001125, 2009.

Schaefer, K, H Lantuit, VE Romanovsky, EAG Schuur, and R Witt .: The impact of the permafrost carbon feedback on global climate, Env. Res. Lett., 9, 085003 (9pp) doi:10.1088/1748-9326/9/8/085003, 2014.

Shiklomanov, N.I.; Streletskiy, D.A.; Nelson, F.E.; Hollister, R.D.; Romanovsky, V.E.; Tweedie, C.E.; Bockheim, J.G.; Brown, J. Decadal variations of active-layer thickness in moisture-controlled landscapes, Barrow, Alaska. *J. Geophys. Res. 115*, G00I04, 2010.

E. A. G. Schuur, A. D. McGuire, C. Schädel, G. Grosse, J. W. Harden, D. J. Hayes, G. Hugelius, C. D. Koven, P. Kuhry, D. M. Lawrence, S. M. Natali, D. Olefeldt, V. E. Romanovsky, K. Schaefer, M. R. Turetsky, C. C. Treat and J. E. Vonk.: Climate change and the permafrost carbon feedback. Nature 520, 171–179. doi:10.1038/nature14338, 2015.

Smith, S., and M.M. Burgess.: Ground Temperature Database for Northern Canada. Geological Survey of Canada Open File Report No. 3954. 28 pages, 2000.

Tarnocai, C., Canadell, J. G., Schuur, E. A. G., Kuhry, P., Mazhitova, G. and Zimov, S.: Soil organic carbon pools in the northern circumpolar permafrost region. *Global Biogeochem. Cycles*, 23, doi:10.1029/2008GB003327, 2009.

Tryon, P., Chapin, F. III.: Tem- perature controls over root growth and root biomass in taiga forest trees. Can. J. For. Res.13:827-33, 1983.

Van Cleve, K.L., Oliver, L., Schlentner, R., Viereck, L. and Dyrness, C.T.:Productivity and nutrient cycling in tiaga forest exosystems. Can. J. For. Res., 13: 747-766, 1983.

Vidale, PL, R Stockli.: Prognostic canopy air space solutions for land surface exchanges, *Theor. Appl. Climatol.*, *80*, 245-257, 2005.

Yi S, Manies K, Harden J and McGuire A D.: Characteristics of organic soil in black spruce forests: implications for the application of land surface and ecosystem models in cold regions Geophys. Res. Lett. 36 L05501, 2009.

Yi, S., A. D. McGuire, E. Kasischke, J. Harden, K. L. Manies, M. Mack, and M. R. Turetsky (2010), A Dynamic organic soil biogeochemical model for simulating the effects of wildfire on soil environmental conditions and carbon dynamics of black spruce forests, J. Geophys. Res., 115, G04015, doi:10.1029/2010JG001302.

Yuan, F., S. Yi, A. D. McGuire, K. H. Johnsen, J. Liang, J. Harden, E. Kasischke, and W. Kurz (2012), Assessment of historical boreal forest C dynamics in Yukon River Basin: Relative roles of warming and fire regime change, Ecol. Appl., 22, 2091-2109.

Wei, Y., Liu, S., Huntzinger, D. N., Michalak, A. M., Viovy, N., Post, W. M., Schwalm, C. R., Schaefer, K., Jacobson, A. R., Lu, C., Tian, H., Ricciuto, D. M., Cook, R. B., Mao, J., and Shi, X.: The North American Carbon Program Multi-scale Synthesis and Terrestrial Model Intercomparison Project: Part 2 - Environmental Driver Data. Geoscientific Model Development, 7, 2875-2893, doi:10.5194/gmd-7-2875-2014, 2014.

Wipf, S., and Rixen, C.: A review of snow manipulation experiments in Arctic and alpine tundra ecosystems. Polar Res 29(1):95–109. doi:10.1111/j.1751-8369.2010.00153.x, 2010.

Zhang, T.: Influence of the seasonal snow cover on the ground thermal regime: An overview, Rev. Geophys., 43, RG4002, doi:10.1029/2004RG000157, 2005.

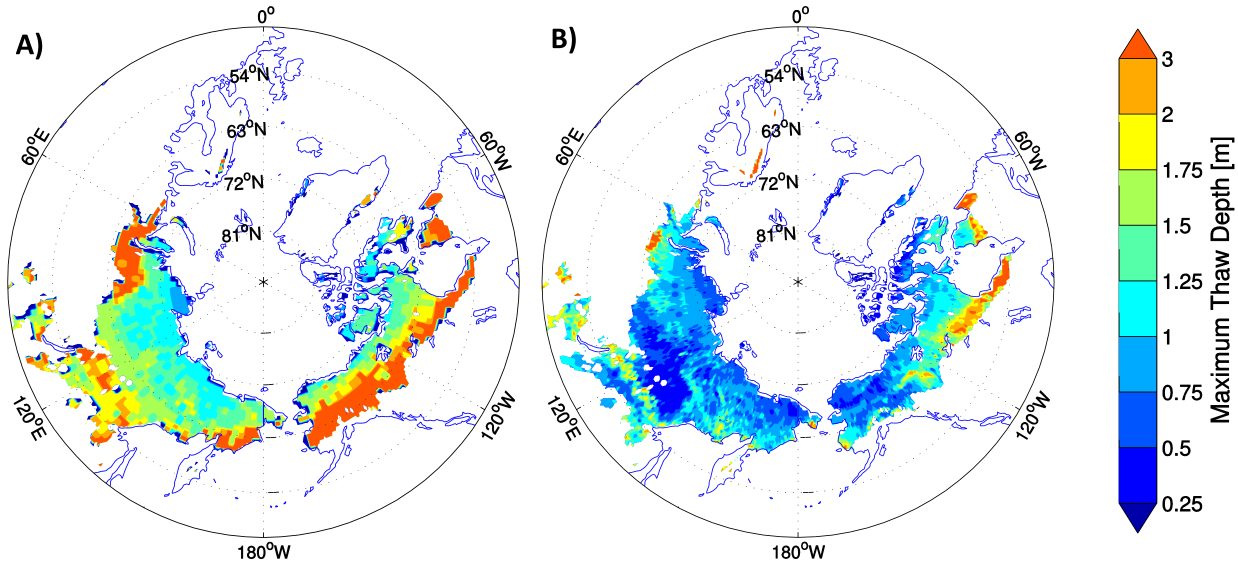

Figure 1. Maximum thaw depth averaged over last five years after spinup from A) Schaefer et al., (2011) and B) this study, in meters.

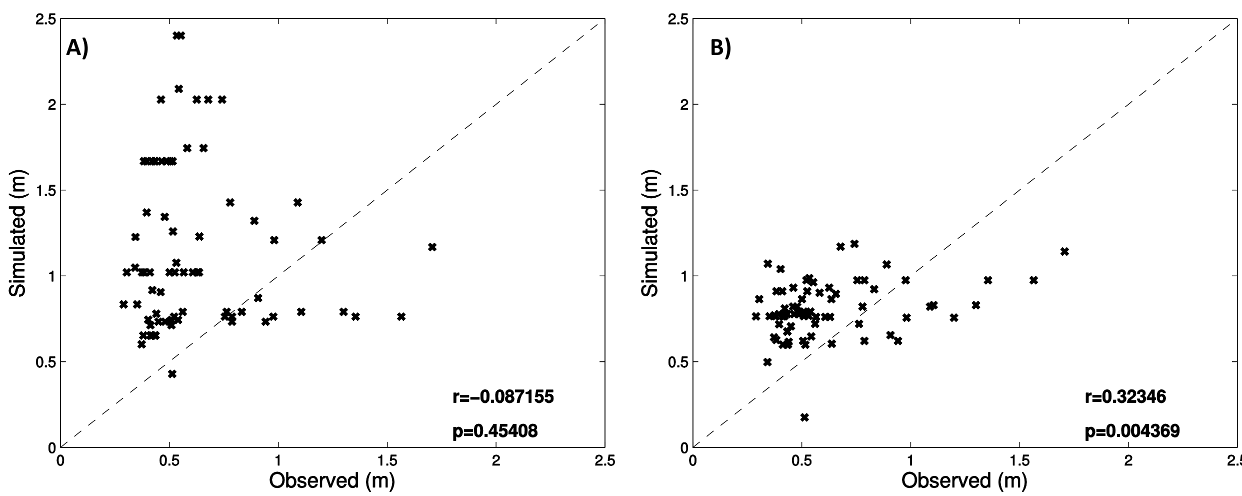

Figure 2. Comparison of the mean active layer thickness (ALT) from 76 Circumpolar Active Layer Monitoring stations with the averaged ALT from last five years after spinup from A) Schaefer et al., (2011) and B) this study. r is a Pearson's correlation coefficient and p is a significance value, $p<0.05$ stands for the 95% of confidence.

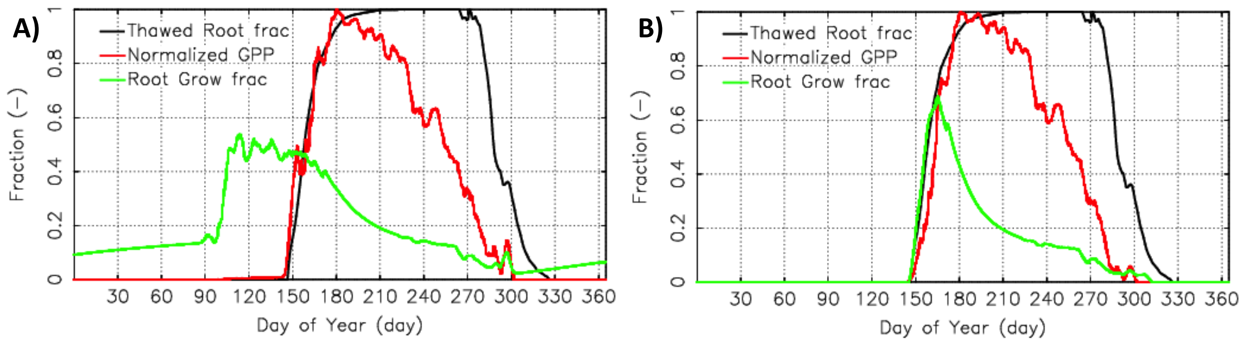

Figure 3: A) and B) root growth without and with the frozen soil constraint on growth.

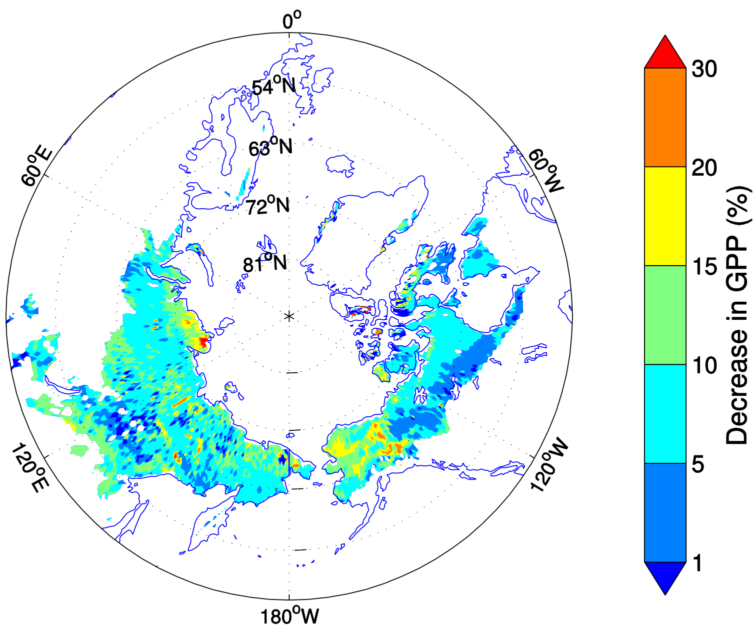

Figure 4. The difference between GPP without and with freezing constraint averaged over ten years.

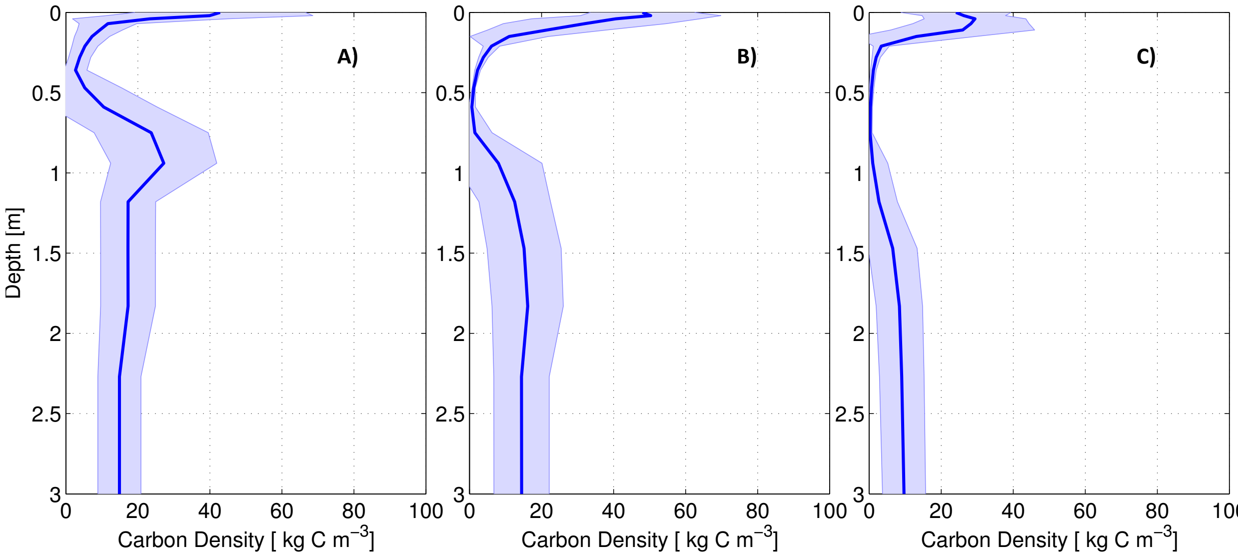

Figure 5. An averaged soil carbon distribution from 200 grid cells A) for the tundra region in continuous permafrost zone, B) for the boreal forest on the boundary between continuous and discontinuous zones, and C) for the low carbon soil at the south border of the discontinuous permafrost zone. The solid blue curve indicates the mean the white blue shading indicate the spread in the soil carbon density.

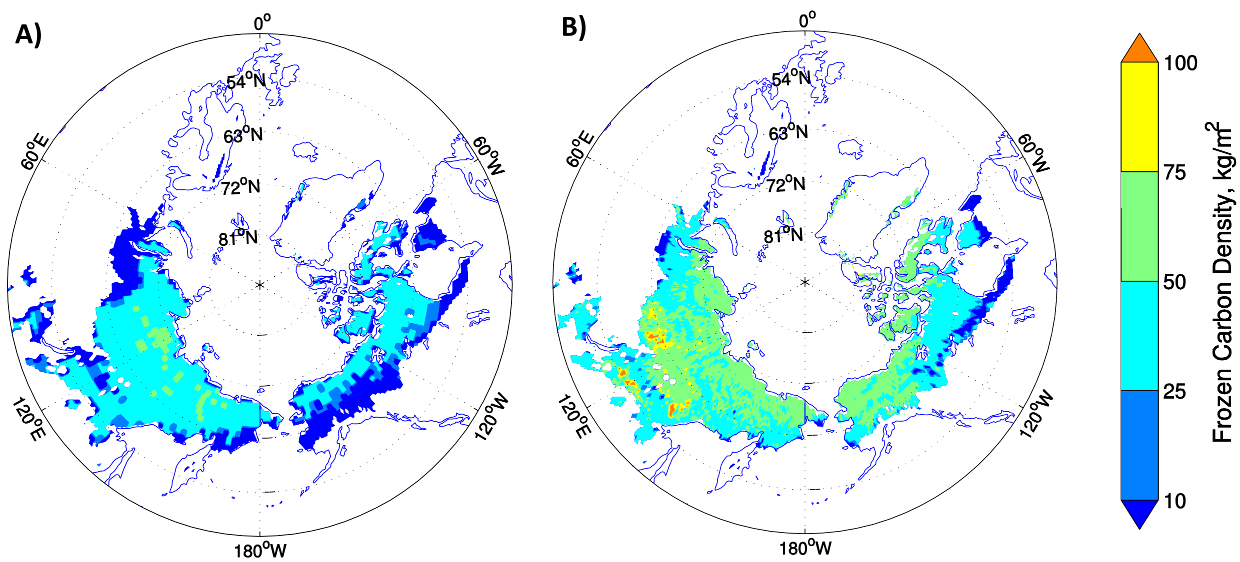

Figure 6. The frozen carbon maps obtained assuming uniform frozen carbon distribution at the initial time step, and averaged over five years at the end of the steady state run: A) from Schaefer et al., (2011), and B) from the current run, correspondingly.

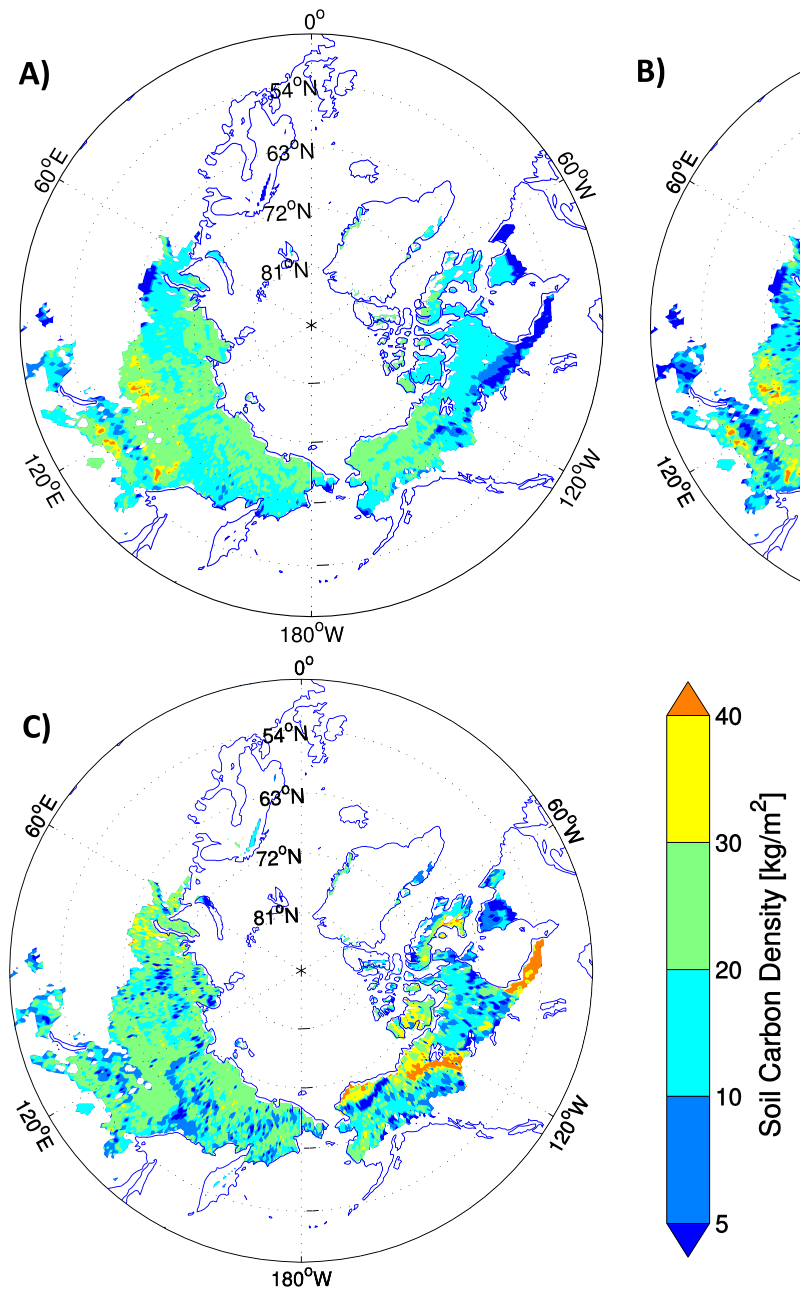

Figure 7. The soil carbon maps averaged over top 3 meters: A) from SiBCASA at the end of the steady state run, with constant permafrost density, B) from SiBCASA at the end of the steady state run, with non-constant permafrost density, and C) from the NCSCDv2, correspondingly.

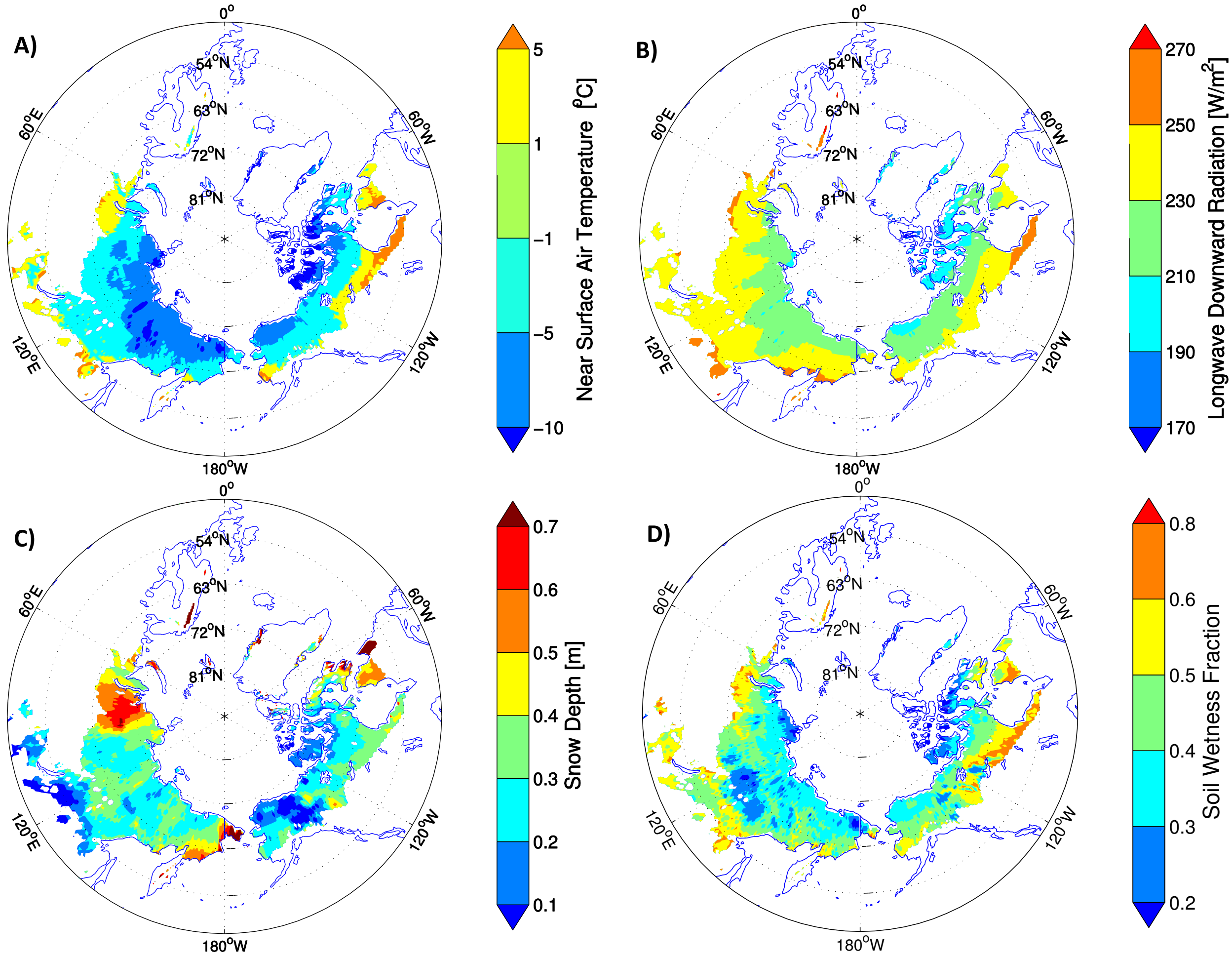

Figure 8. A) The near air temperature for averaged over first two month of the fall season. B) The down-welling long-wave radiation, averaged yearly over 10 years. C) The maximum snow depth obtained over 10 years for the steady state run, and D) the soil wetness fraction (dimensionless fraction of 1), representing overall near-surface soil wetness, averaged yearly over 10 years.

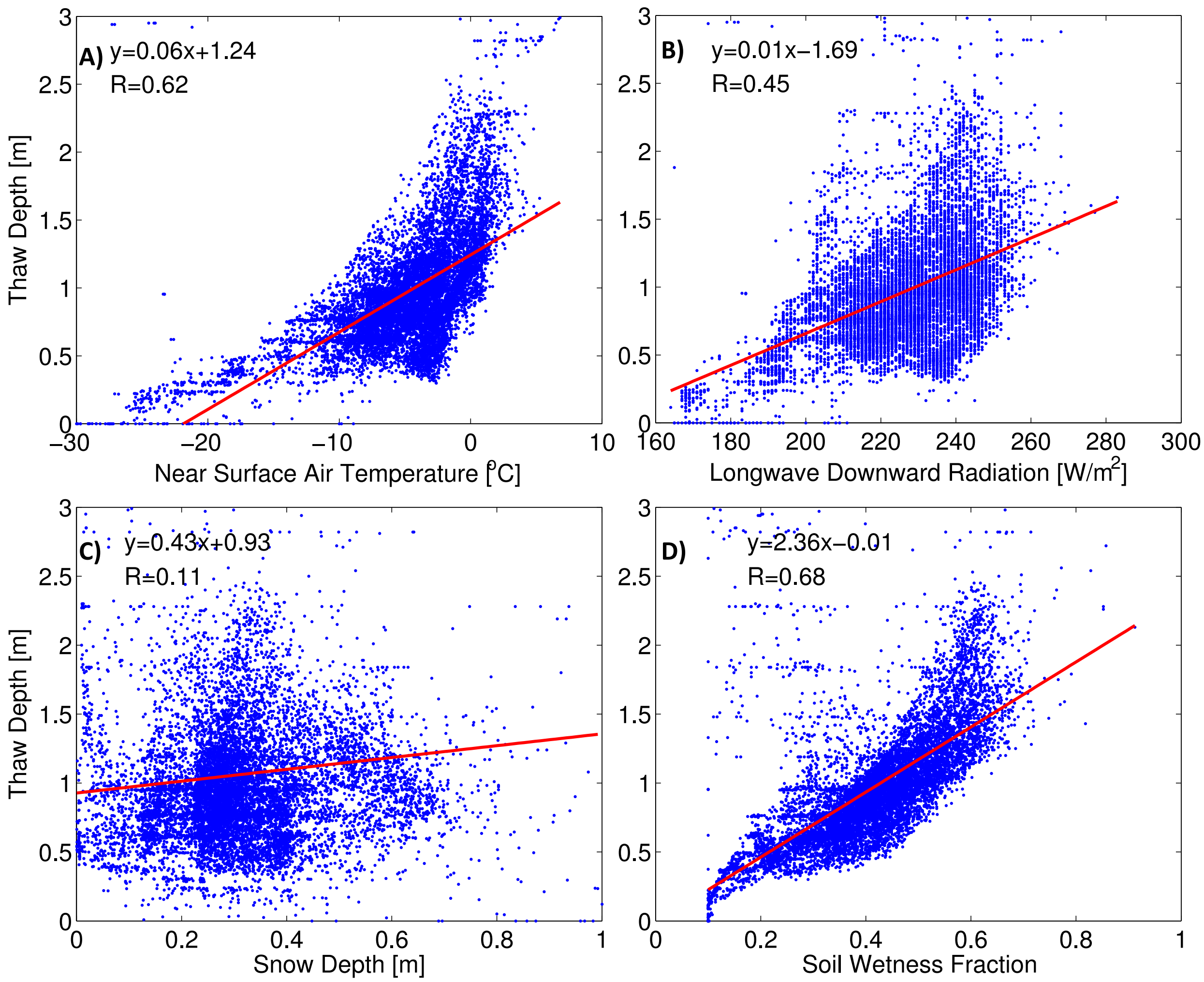

Figure 9. The correlation between ALT and: A) near air temperature for averaged over first two month of the fall season, and B) the down-welling long-wave radiation, averaged yearly over 10 years. C) the maximum snow depth over 10 years for the steady state run, and D) the soil wetness fraction, averaged yearly over 10 years.